J. Phys. D: Appl. Phys. **22** (1989) 1456–1463. Printed in the UK

Double layers formed by ion-beam injection in a double-plasma device

James C Johnson, Robert L Merlino and Nicola D'Angelo

Department of Physics and Astronomy, The University of Iowa, Iowa City, IA 52242-1479, USA

Received 9 March 1989, in final form 8 May 1989

Abstract. Electric double layers have been produced in a double-plasma device by the injection of an ion beam into a target plasma. A longitudinal magnetic field is present, of sufficient strength to magnetise the electrons. The double layers occur if the electron density in the target plasma is not sufficient to neutralise the injected space charge. The strength and axial position of the double layers can be controlled by varying the plasma density in the target, the ion-beam density, the neutral pressure, or the magnetic field strength. The double layers seem to form at a position where the ion and electron fluxes satisfy, approximately, the Langmuir condition. The electric fields in the double layers are compared to the values predicted by the original Langmuir theory, later modified by Andrews and Allen to include the effects of reflected particles and initial velocities.

1. Introduction

In this paper we report observations of electric double layers in a double-plasma (DP) device. The double-plasma device was introduced in 1969 by Taylor, Ikezi and MacKenzie (Taylor *et al* 1969, 1972) and was used primarily to produce large planar ion beams. Typically, these devices consist of two identical, but electrically independent, vacuum chambers, separated by a fine mesh grid. Plasma is produced in each chamber by a hot-filament discharge, operating typically at (argon) pressures in the range of 10^{-5}–10^{-3} Torr (1 Torr = 133 Pa). The resulting plasma densities and temperatures are in the range $n_e \sim 10^7$–10^{10} cm^{-3} and $T_e \sim 10\, T_i \simeq 2$ eV. The separation grid is held at a sufficiently negative bias to prevent electrons from either chamber from entering into the other chamber. In one chamber, designated the 'driver', the anode may be biased with respect to ground so as to control the driver space potential. The walls of the other chamber, the 'target', are grounded, with the plasma space potential, determined by the target discharge conditions, usually a few volts positive. When a positive bias is applied to the driver anode, a planar ion beam is injected through the grid into the target region. The kinetic energy of the ion beam is given by the difference in space potentials between the driver and target, and is variable, typically up to several tens of volts.

The discharge in the target provides the necessary electrons to neutralise the positive space charge of the injected ion beam. If a sufficient number of target electrons is provided, the target space potential remains near ground (within a few volts) and is nearly uniform axially, so that an ion beam of well defined energy, $eV_{beam} \simeq e(V_{SD} - V_{ST})$, can be injected, where $V_{SD/T}$ is the driver/target space potential.

We have conducted a series of experiments in our DP device under conditions in which the injected ion beams were only partially space-charge neutralised. Under these circumstances we found that the space potential in the target is no longer spatially uniform along the direction of ion-beam injection, and an electric double layer forms, separating a region of high from one of low plasma potential. The axial location of the double layer depends, in part, on the relative magnitudes of the driver and target discharge currents. When the target discharge current is high enough so that target electrons are plentiful, normal DP device conditions are recovered and no double layers are formed.

There have been a few investigations of double-layer formation in double-plasma devices. (A recent and comprehensive review of laboratory double-layer experiments is given by Hershkowitz (1985).) For example, Quon and Wong (1976) produced double layers by injecting *electrons* from the driver into the target region of a double-plasma device. Similar experiments were performed by Mattoo *et al* (1980) and Sekar and Saxena (1985). Stenzel *et al* (1981) investigated the formation of double layers by injecting an ion beam into the sheath of a positively biased electrode in a magnetic dipole configuration. In the latter case, however, the positive space-charge layer arose due to the reflection of the beam ions in the electron-rich sheath. This mechanism of double-layer formation has some similarities to ionisation-produced double

0022-3727/89/101456 + 08 $02.50

layers near a positive plate in a weakly ionised plasma (Torvén and Andersson 1979, Cartier and Merlino 1987). The double layers which we discuss here are also similar to double layers produced by applying a potential difference between two independently produced plasmas (see, for example, Torvén 1982, Sato *et al* 1981, Guyot and Hollenstein 1983). In our configuration, however, the two source plasmas are separated by an electron-reflecting grid which prevents large current flow between the two sources. The double layers which we have studied are generally characterised by $e\Delta V/kT_e \sim 5$–10 and $\Delta L/\lambda_D \sim 10$–$100$, where ΔV and ΔL are the potential drop and thickness of the double layers, respectively, and λ_D is the Debye length in the target plasma. We have been able to produce double layers over a wide range of neutral pressures, $\approx 10^{-5}$–10^{-2} Torr, in which the ion–neutral charge exchange mean free path, λ_{ce}, covers the range $\lambda_{ce} > \Delta L$ and $\lambda_{ce} < \Delta L$. In all cases, however, the mean free paths for electron–neutral collisions exceeds ΔL. A longitudinal magnetic field sufficiently strong to magnetise the electrons, but not the ions, is also provided in our device.

Following these introductory remarks we give, in § 2, a description of the experimental device and the diagnostics used to determine the various plasma parameters. The experimental results are presented in § 3. In § 4 we compare these results with the original double-layer model as proposed by Langmuir in 1929 and extended by Andrews and Allen in 1971. A summary of our conclusions is given in § 5.

2. Experimental method

A schematic diagram of the DP device and the associated electrical circuits is shown in figure 1(*a*). Figure 1(*b*) shows an axial profile of the longitudinal magnetic field (on-axis).

Plasma is produced in the end chambers by independent hot filament discharges, usually in argon at pressures in the range of 10^{-5}–10^{-2} Torr (1.33×10^{-3} Pa–1.33 Pa). Typically, the driver discharge operates at a discharge voltage $V_{dD} \simeq 40$ V and current $I_{dD} \simeq 2.5$ A, while the target discharge parameters are $V_{dT} \simeq 30$ V, $I_{dT} \simeq 2.5$ A. The electron density in the driver is $\sim 10^9$–10^{10} cm^{-3}. For most of the experiments described here, the magnetic field in the central region was less than 20 G. Since the filaments are located in the fringing magnetic field region, the plasma remains reasonably uniform even when the magnetic field is raised to ~100 G in the central region.

The driver anode is a cylindrical 'cage' which is electrically isolated from the chamber walls. The driver region and target region are separated by a fine mesh grid (140 lines per inch), located at $Z = 0$. When the cage bias V_c is applied, an ion beam is injected through the grid, from the driver into the target. Further details of the 'normal' operation of the DP device are given in Johnson *et al* (1988).

The plasma properties are determined using Langmuir probes (collecting and emitting) and a gridded ion-energy analyser. The collecting Langmuir probes are used to determine the electron density n_e and tem-

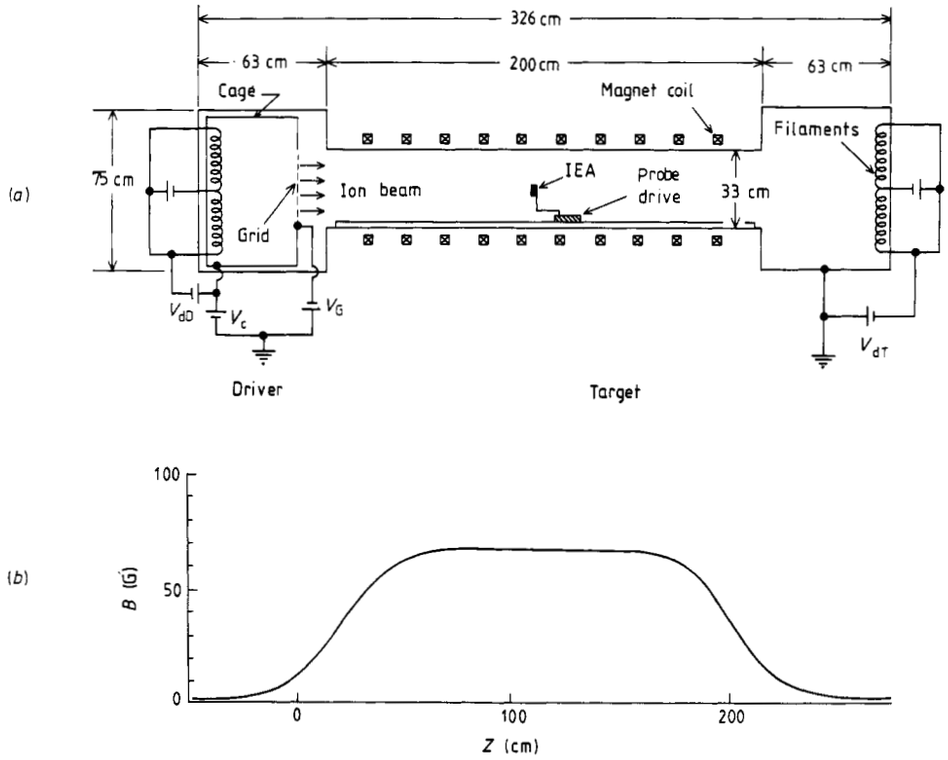

Figure 1. (*a*) Schematic diagram of the experimental apparatus. (*b*) Axial profile of the magnetic field.

perature T_e. These probes are usually tantalum discs 0.5–1 cm in diameter. Occasionally, double-sided (back-to-back) Langmuir probes are used to infer further characteristics of the electron velocity distribution. The ion-energy analysers are used to determine the flux and kinetic energy of the ion beams and also the flux and temperatures of the thermal ions. The plasma space potential is inferred from measurements of the floating potential of an emissive probe. This probe consists of a 0.025 mm diameter tungsten wire, approximately 5 mm in length, heated with a direct current provided by a 12 V automobile battery. The floating potential of the probe is measured using a high-input resistance ($>10^{12}\ \Omega$) voltmeter. The operating point (heating current) of the emissive probe is determined by observing the full probe characteristic (I–V curve) and adjusting the heating current until the floating potential is sufficiently close to the space potential. For the relatively strong double layers which were studied, the floating potential is usually within one volt of the actual space potential. The probes or the ion-energy analyser can be mounted on a probe drive mechanism so that axial and radial scans of the plasma can be made in the central region (~160 cm long) of the device.

3. Experimental results

The presentation of the results will be divided into a number of subsections, each describing various aspects of the double layers.

3.1. Formation of double layers

Our observations of double layers developed from a series of measurements of the axial profile of the space potential in the DP device. The DP device was operated in the usual mode in which an ion beam was injected through the grid, from the driver to the target, by raising the driver anode (cage) potential, V_c, above ground. Figure 2 shows axial profiles of the potential for several values of the argon neutral pressure at fixed

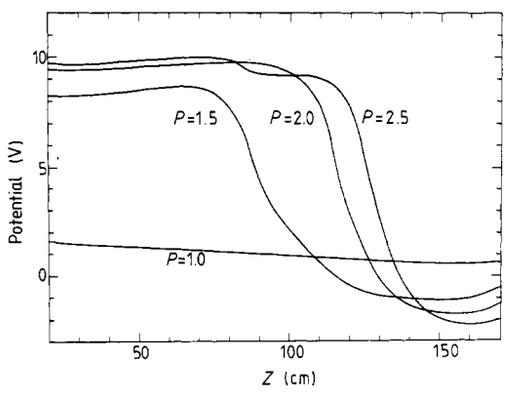

Figure 2. Axial potential profiles for various neutral pressures (in units of 10^{-3} Torr). $B = 13$ G, $I_{dT} \simeq I_{dD} \simeq 2.5$ A, $V_c = 20$ V.

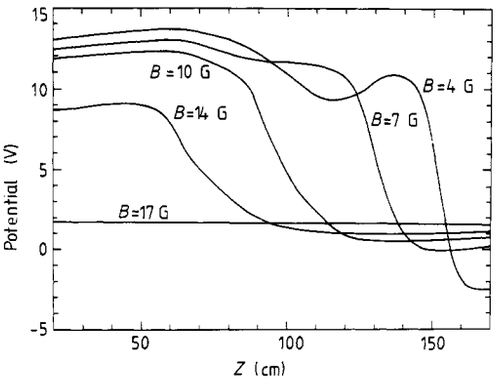

Figure 3. Axial potential profiles for various magnetic fields. $p \simeq 1 \times 10^{-3}$ Torr, $I_{dT} \simeq I_{dD} \simeq 2.5$ A, $V_c = 15$ V.

driver and target discharge currents, and for $B = 14$ G. All axial distances (Z) are measured from the grid, the ion-beam injection point. For a neutral pressure of 1.0×10^{-3} Torr, the potential is fairly uniform in the target region. When the neutral pressure is raised, however, to 1.5×10^{-3} Torr a double layer forms at ~90 cm. A further increase in the neutral pressure causes the double layer to be formed farther from the grid. A similar behaviour is observed as the magnetic field is varied, as shown in figure 3, at a fixed pressure of $\simeq 1 \times 10^{-3}$ Torr and a somewhat lower cage voltage. In this case the double layers are formed when B is lowered to about 14 G. As B is reduced the double layers appear farther from the grid. The effect of the neutral pressure and magnetic field strength on the formation of double layers has been investigated over

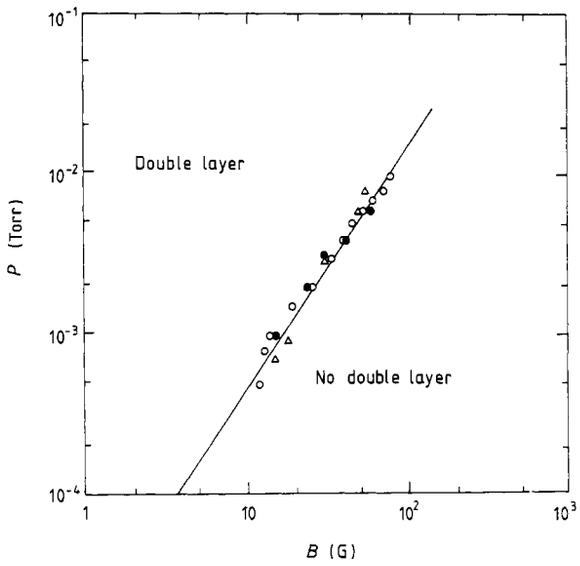

Figure 4. Pressure and magnetic field combinations for double layer/no double layer transitions. Double layers were observed for p, B combinations lying to the left of the diagonal line. The data points are the maximum magnetic field values for which a double layer was present at a given pressure. The various symbols correspond to different discharge conditions.

a wide range of these parameters. The results are summarised in figure 4 which shows the p–B combinations for which double layer/no double layer transitions occur in our device. The various points in this figure correspond to different discharge conditions. For example, at a pressure of 1×10^{-3} Torr, a double layer will be formed only for magnetic field strengths below about 15 G.

The formation and properties of the double layers are also dependent on the cage voltage (driver anode potential) as shown in figure 5(a). As V_c is increased the potential in the target near the grid rises, and a double layer is formed at increasing axial distances from the grid. For $V_c \geqslant 10$ V, very little change in the double layer is observed (either in position or strength). The behaviour of the double layers as V_c is varied can be understood, in part, on the basis of the additional data in figure 5(b), which show the dependence of the driver cage current on V_c. This current is approximately equal to the ion-beam current into the target. We see that for V_c up to $\approx$10 V, I_{cage} increases sharply with V_c. For higher values of V_c, I_{cage} shows only a very gradual variation. Thus, the behaviour of the potential in figure 5(a) as V_c is increased can be attributed to an increase in the ion space charge injected into the target.

These data suggest that double layers may be present in a DP device whenever an insufficient flux of electrons is available from the target discharge to neutralise the positive space charge of the injected ion beam. For pressures $\sim 10^{-3}$ Torr the mean free path for ion–neutral charge exchange is $\lambda_{ce} \sim 6$ cm, so the injected ion beam is rapidly converted into slow thermal ions after injection into the target. The electron flux toward the grid from the target plasma is reduced as the pressure is increased, due to electron–neutral collisions. For $p \sim 10^{-3}$ Torr the mean free path for electron–neutral collisions is $\lambda_{en} \simeq 1/N\sigma \simeq 1/(3 \times 10^{13}\,\mathrm{cm}^{-3} \times 5 \times 10^{-16}\,\mathrm{cm}^2) \sim 65$ cm, which is shorter than the length of the target chamber. The electron flux near the double layer is also affected by the magnetic field. At higher magnetic fields the electrons are better confined so that sufficient negative space charge is available to neutralise the ion space charge, and no double layers are formed. In the next subsection, the effect of varying the driver and target discharge currents will be considered.

3.2. Axial potential profiles for various driver and target discharge conditions

The role of the target electrons in neutralising the injected ion space charge was studied by holding constant the driver discharge conditions, pressure and magnetic field and varying the target discharge current. The target filaments were operated in the space-charge-limited mode so the discharge current could be varied by varying the discharge voltage. The results are shown in figure 6. For a sufficiently high target discharge current (2.80 A), no double layers are formed (we verified also that the potential was essentially flat to within 5 mm of the grid). When the electron flux is reduced, by lowering I_{dT}, the double layers appear farther and farther from the grid. A similar behaviour is observed when the target discharge conditions are held constant but the driver conditions are varied as seen in figure 7. By varying the driver discharge current, we can control the injected ion flux. As the ion flux is

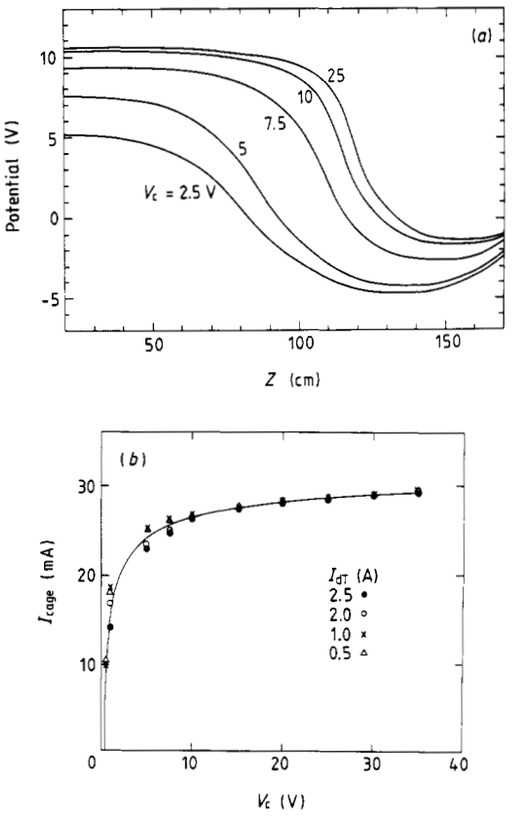

Figure 5. (a) Axial potential profiles for various cage voltages. (b) Dependence of the cage current on cage voltage. $p \simeq 2 \times 10^{-3}$ Torr, $B = 13$ G, $I_{dT} \simeq I_{dD} \simeq 2.5$ A.

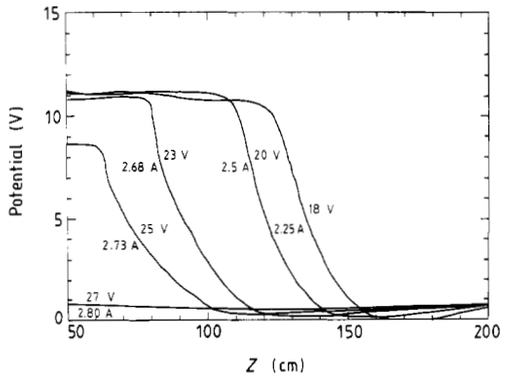

Figure 6. Axial potential profiles for various target discharge conditions. $p \simeq 2 \times 10^{-3}$ Torr, $B = 13$ G, $I_{dD} \simeq 2.5$ A.

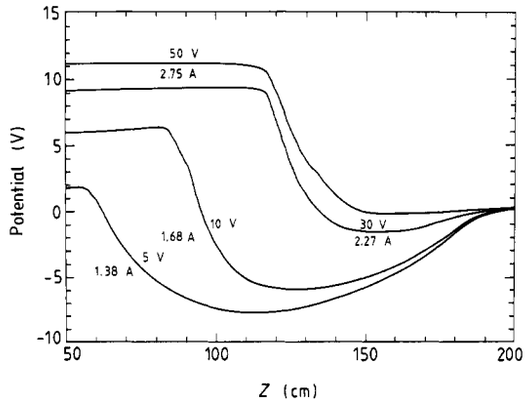

Figure 7. Axial potential profiles for various driver discharge conditions. $p \simeq 2 \times 10^{-3}$ Torr, $B \simeq 13$ G, $I_{dT} \simeq 2.5$ A.

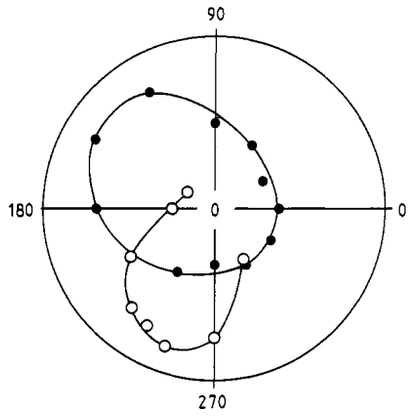

Figure 9. Angular distribution of the thermal ion flux at $R = -8$ cm (●) and $R = +10$ cm (○), corresponding to the potential contours of figure 8. The driver is on the left-hand side in this figure.

increased, the double layer forms farther from the grid. If the driver discharge is turned off, the potential in the target decreases monotonically toward the grid. When the ions are injected, however, the potential near the grid is lifted and a double layer is formed. At lower driver discharge currents, a negative potential 'well' is formed which limits the electron flux to the double layer from the low-potential side.

3.3. Two-dimensional potential profiles and ion losses

Figure 8 shows equipotential contours, in the R–Z plane, for a double layer obtained under the conditions $p \simeq 3 \times 10^{-4}$ Torr and $B = 7$ G. The double-layer potential transition occurs axially from about $Z = 108$ cm to about $Z = 125$ cm. The potential contours shown vary from 16 to 4 V, in 4 V increments. The double layers are at least two dimensional, since substantial radial electric fields are present over extended regions. These radial electric fields should give rise to substantial ion losses. A radially outward ion flow was observed using a small ion-energy analyser which could be rotated about the vertical axis. Figure 9 shows polar plots of the ion flux at $Z = 111$ cm, and at two radial locations on either side of the axis. For $R = +10$ cm the flux peaks at approximately 250°, while for $R = -8$ cm the maximum flux occurs at ~135°. The angular distributions of these fluxes are qualitatively what one would expect given the radial electric fields in figure 8.

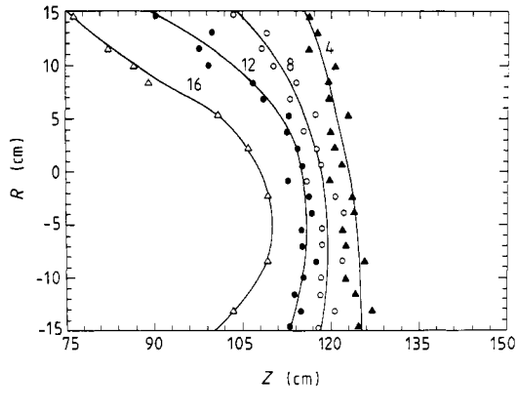

Figure 8. Equipotential contours in the R–Z plane. $p \simeq 3 \times 10^{-4}$ Torr, $B = 7$ G, $I_{dT} \simeq 2$ A, $I_{dD} \simeq 4$ A, $V_c = 15$ V.

3.4. Electron and ion flux measurements

The observed shift in the position of the double layer as the neutral pressure (figure 2) is varied was further investigated by obtaining measurements of the axial profiles of the electron and ion flux. Measurements of the electron flux from the target plasma toward the driver were obtained using a double-sided Langmuir probe in which the electron current to either side could be measured independently. The ion flux measurements were made using the ion-energy analyser facing the high-potential side. Axial profiles of the electron and ion flux for two values of the neutral pressure are shown in figures 10(*a*) and (*b*); all other conditions correspond to those of figure 2. In figure 10(*a*) we see clearly that at a given Z the electron flux is reduced when the neutral pressure is increased. Figure 10(*b*) shows the large reduction in ion flux near the double layer presumably due to the large radial ion losses.

3.5. Electron and ion temperatures

To complete our presentation of the experimental results we include some measurements of electron and ion temperatures in the presence of the double layer. The electron temperatures were obtained using the double-sided Langmuir probe, while the ion temperatures were measured with the ion-energy analyser.

A plot of the electron temperatures at various axial positions for the double layer corresponding to the 1.5×10^{-3} Torr case of figure 2 is shown in figure 11. Within the high-potential region $Z \leqslant 70$ cm, a two-

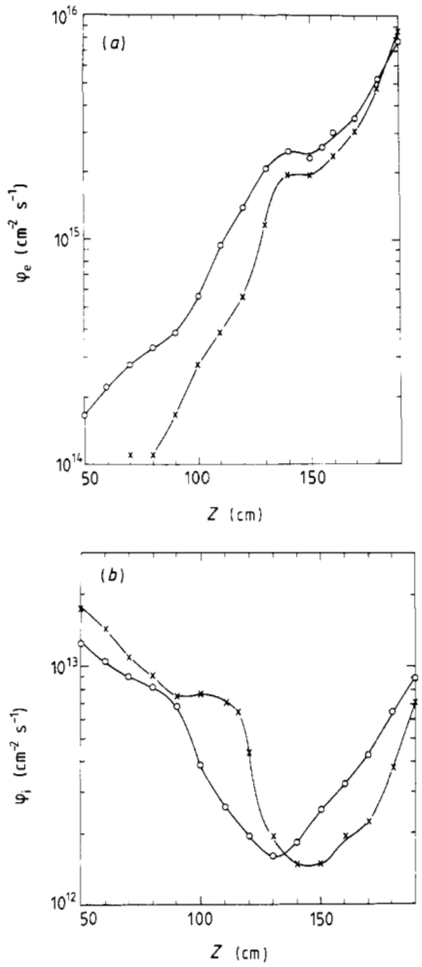

Figure 10. Axial profiles of the electron flux (*a*) and ion flux (*b*) for two values of the neutral pressure (○, $p = 1.7 \times 10^{-3}$ Torr; ×, $p = 2.2 \times 10^{-3}$ Torr). $B = 13$ G.

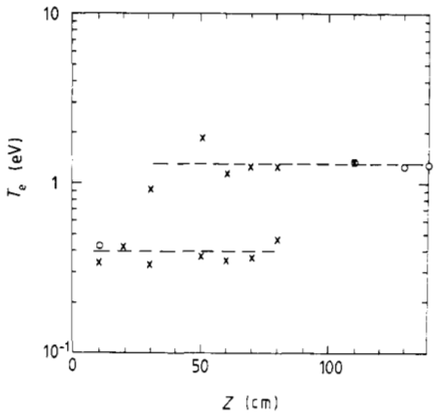

Figure 11. Axial profiles of electron temperatures; probe facing the driver (×) and probe facing the target (○). $p = 1.5 \times 10^{-3}$ Torr, $B = 13$ G, $I_{dT} = I_{dD} \simeq 2.5$ A, $V_c = 15$ V.

temperature distribution was found, while only a single-temperature electron distribution was present within the double layer and in the low-potential region. The presence of a relatively cold (~0.4 eV) electron population within the high-potential region indicates

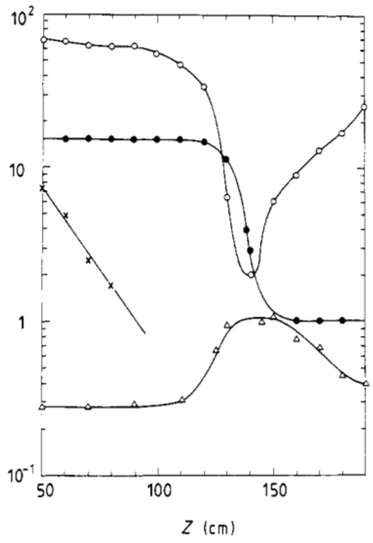

Figure 12. Axial profiles of ion-beam flux (×, arbitrary units), thermal ion flux (○, arbitrary units), space potential (●, V) and ion temperature (△, eV). $p \simeq 3 \times 10^{-4}$ Torr, $B = 7$ G, $I_{dT} = I_{dD} \simeq 2.5$ A, $V_c = 20$ V.

that these electrons are confined for a long time compared to a typical electron–neutral collision time, so that they are effectively cooled by electron–neutral collisions, but not quite to the neutral gas temperature (~0.03 eV). In attempting to understand the flow of electrons through the double layer, we must keep in mind that these electrons cannot escape axially since they will be trapped between the (negative) grid and the double layer. However, even though they are effectively confined axially, they may eventually diffuse radially outward due to the inward density gradient. This outward diffusion will be slowed down by the radial electric field.

We have also observed a heating of the ions as they pass through the double layer. This effect is presented in figure 12 which shows axial plots of the ion-beam flux, thermal ion flux, space potential and ion temperature for a double layer obtained at a pressure of 3×10^{-4} Torr. Under these conditions the mean free path for ion–neutral charge exchange collisions is comparable to the width of the double layer ≃20–30 cm. The ion beam injected into the target is rapidly attenuated through charge exchange resulting in a thermal ion distribution with $T_i \lesssim 0.3$ eV. Ions which fall down the potential hill of the double layer do not experience a 'free' acceleration but collide frequently, leading to an effective 'heating' of the ions to about 1 eV. These ions continue to undergo charge exchange collisions, cooling back down to ≃0.4 eV on the low-potential side.

4. Discussion

Our discussion of the experimental results will concentrate on the questions of (i) where the double layers

are formed, and (ii) how large are the resulting electric fields.

With regard to point (i), Langmuir (1929) showed, in his pioneering work on the double space-charge sheath, that the ratio of electron-to-ion flux at the double layer is given by

$$\frac{\varphi_e}{\varphi_i} = \left(\frac{m_i}{m_e}\right)^{1/2}. \quad (1)$$

Langmuir's theory has been summarised nicely by Lars Block (1972), who further developed the model.

Langmuir's analysis assumes a double layer infinitely extended in, say, the x and y directions, with cold plasmas on either side of the double layer. The double-layer potential drop occurs along the Z axis with the potential V_0 at $Z = 0$ and $V = 0$ at $Z = Z_1$. The electron and ion flux at the double layer are φ_e and φ_i, respectively. By applying conservation of energy and particle flux, Poisson's equation, with the requirement that $E = 0$ at $Z = Z_1$, may be integrated to obtain the electric field

$$E^2 = C^2\{\varphi_e V^{1/2} + \mu\varphi_i[(V_0 - V)^{1/2} - V_0^{1/2}]\} \quad (2)$$

where $C^2 = (8em_e/\varepsilon_0^2)^{1/2}$ and $\mu = (m_i/m_e)^{1/2}$.

The Langmuir condition $\varphi_e = \mu\varphi_i$ follows from the boundary condition $E = 0$ at $V = V_0$ ($Z = 0$). The maximum value of E occurs at $V = \frac{1}{2}V_0$ and, when the Langmuir condition is applied, can be shown to scale as

$$E_{max} \sim \varphi_i^{1/2} V_0^{1/4}. \quad (3)$$

The effect of the reflected particles and the initial velocities of the accelerated particles on the electric field, point (ii) above, was analysed by Andrews and Allen (1971). The accelerated particles were assumed to be monoenergetic. Their analysis showed that the inclusion of reflected particles and initial velocities in the Langmuir model can have a large effect on the ratio of electron and ion currents through the double layer. They expressed their 'modified' Langmuir condition as $\varphi_e/\varphi_i = \alpha(m_i/m_e)^{1/2}$, where α is a numerically computed parameter which depends on the temperatures of particles entering the double layer. For our particular conditions this factor $\alpha \sim 0.5$.

From the electron and ion flux measurements presented in figure 10, we have constructed plots of the electron-to-ion flux ratio for two values of the argon pressure. These plots are shown in figure 13. The horizontal lines in figure 13 correspond to the flux ratios as predicted by Langmuir ($\alpha = 1$) and by the theory of Andrews and Allen ($\alpha = 0.5$). The approximate locations of the double layers are indicated by the cross-hatched regions. These plots give quantitative evidence that the double layers form at positions where the flux ratio φ_e/φ_i assumes a particular value, $\beta(m_i/m_e)^{1/2}$, where $\beta \approx 0.5$–1. A similar analysis performed on sets of data obtained at a fixed argon pressure but at two different values of the magnetic field leads to the same conclusion.

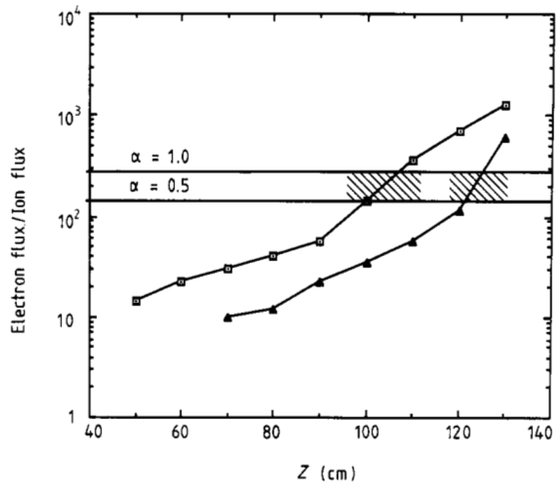

Figure 13. Axial profiles of the electron-to-ion flux ratio, for two values of the argon pressure (□, p = 1.7 mTorr; ▲, p = 2.2 mTorr), obtained from the data of figure 10. The horizontal lines are the predicted flux ratios corresponding to the Langmuir condition (α = 1) and 'modified' Langmuir condition (α = 0.5) of Andrews and Allen. The cross-hatched regions mark the approximate positions of the two double layers.

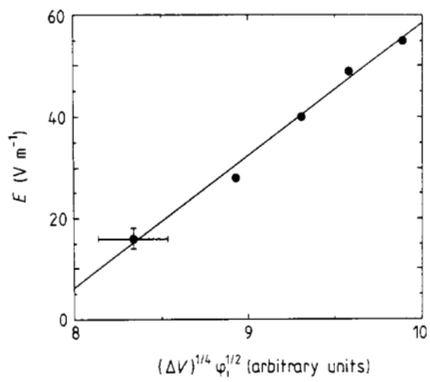

Figure 14. Scaling of the maximum double-layer electric field with total voltage drop and ion flux. p = 2 mTorr, B = 13 G.

With regard to point (ii), the question of the double-layer electric fields, we first checked the scaling of the electric fields as predicted by equation (3). This was done for the series of double layers of figure 5(*a*), with $V_0(=\Delta V)$ taken to be the total potential drop across the double layer. The ion flux was estimated from the cage currents of figure 5(*b*). Over the somewhat limited range of the parameters, this scaling seems to be appropriate, as indicated in figure 14.

Although the scaling of the experimental data is reasonably consistent with Langmuir's analysis, the actual measured values of E are on the order of 10–30 times less than the values given by equation (2). In attempting to reconcile this discrepancy, we need to keep in mind the several significant differences between the experimental conditions and assumptions of the theory, e.g. (*a*) the theory is for infinite planar

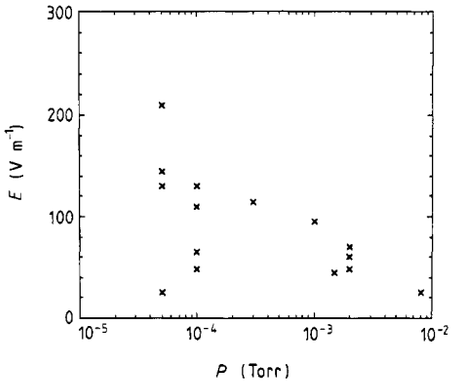

Figure 15. Maximum double-layer electric fields versus neutral pressure.

double layers, and the actual double layers are at least two dimensional; (*b*) the theory assumes cold ($T = 0$) plasmas on either side of the double layer and (*c*) the theory is collisionless, whereas in our experiments the mean free path for ion–neutral collisions is often less than or comparable with the width of the double layer.

With respect to point (*c*), the data do show that weaker double layers (lower *E*s) are obtained at higher neutral pressures. Figure 15 shows a scatter plot of the measured *E*-fields for various double layers as a function of pressure. There seems to be a clear trend toward stronger double layers at lower pressures. This trend is also in line with the experiments of Torvén (1982), where even stronger double layers were obtained at very low neutral pressures.

Andrews and Allen also provide a normalised potential profile (see their figure 6) from which the electric field can be estimated. Using experimental parameters appropriate to our conditions, their theory predicts an $E_{max} \approx 500$–$800\ V\ m^{-1}$, well below the value of $\approx 2700\ V\ m^{-1}$ from the Langmuir model which excludes reflected particles and initial velocities. The values predicted by the more realistic analysis are much closer to the measured values, although still somewhat higher. This extended model, however, excludes magnetic field effects, collisions and ionisation in the double layer.

5. Conclusions

Electric double layers have been produced by the injection of ions into a low-density, partially ionised plasma. The experiments were conducted in a longitudinal magnetic field, although only the electrons were well magnetised. The double layers form at axial locations where the electron-to-ion-flux ratio obeys approximately the Langmuir condition. If the external parameters are varied, the double layers always relocate to a new position where the Langmuir condition can again be satisfied. The scaling of the double-layer electric field with the potential drop and ion flux is consistent with the double-sheath model of Langmuir. The measured values of these electric fields, however, can depart significantly from the 'Langmuir value'. This discrepancy is largely reduced when the effects of initial particle velocities and reflected particles are included in the analysis (Andrews and Allen 1971). We obtain reasonably good agreement between our observations and the simple basic Langmuir model (as extended by Andrews and Allen), even though the effects of collisions with the neutrals, which are not included in the theory, may be important in our experiments.

Acknowledgments

We wish to thank Tim Clark and Al Scheller for their enthusiastic support in the design and construction of the double-plasma device. This work was supported by the United States Office of Naval Research and by NASA.

References

Andrews J G and Allen J E 1971 *Proc. R. Soc.* A **320** 459
Block L 1972 *Cosmic Electrodyn.* **3** 349
Cartier S L and Merlino R L 1987 *Phys. Fluids* **30** 2549
Guyot M and Hollenstein Ch 1983 *Phys. Fluids* **26** 1596
Hershkowitz N 1985 *Space Sci. Rev.* **41** 351
Johnson J C, D'Angelo N and Merlino R L 1988 *IEEE Trans. Plasma Sci.* **PS-16** 590
Langmuir I 1929 *Phys. Rev.* **33** 954
Mattoo S K, Saxena Y C and Sekar A N 1980 *Pramana* **15** 525
Quon B H and Wong A Y 1976 *Phys. Rev. Lett.* **37** 1393
Sato N, Hatakeyama R, Iizuka S, Mieno T, Saeki K, Rasmussen J J and Michelson P 1981 *Phys. Rev. Lett.* **46** 1330
Sekar A N and Saxena Y C 1985 *Plasma Phys. Controlled Fusion* **27** 673
Stenzel R L, Ooyama M and Nakamura Y 1981 *Phys. Fluids* **24** 708
Taylor R J, Ikezi H and MacKenzie K R 1969 *Proc. Int. Conf. Phys. Quiescent Plasmas, Paris, 8–13 September 1969* pp 57–66
Taylor R J, MacKenzie K R and Ikezi H 1972 *Rev. Sci. Instrum.* **43** 1675
Torvén S 1982 *J. Phys. D: Appl. Phys.* **15** 1943
Torvén S and Andersson D 1979 *J. Phys. D: Appl. Phys.* **12** 717